database (http://ifr48.timone.univ-mrs.fr/MST_BHenselae/mst). A neighbor-joining tree was reconstructed from the concatenated MLST allele sequences of 14 previously reported STs (Iredell *et al.*, 2003; Arvand *et al.*, 2007) and the novel ST-15 using Kimura 2-parameter distance measures as implemented in MEGA4 (Tamura *et al.*, 2007).

### Nucleotide sequence accession numbers

Newly encountered sequences have been submitted to DDBJ under the following accession numbers: AB525232, *rpoB* allele 5 (YC-073); AB525233, S1 genotype 11 (YC-053); and AB534165, S1 genotype 12 (YC-012 and YC-013).

## Results and discussion

MLST analysis detected three STs in 55 human and cat *B. henselae* strains. Intriguingly, 94.5% (52/55) of *B. henselae* strains including all 24 human clinical specimens were assigned to ST-1, and only three cat isolates were assigned to other STs (Table 1). In isolate YC-073, a new allele was found in *rpoB*, which consisted of a single nucleotide variation (G instead of A) at position 711 784 of the *B. henselae* Houston-1 chromosome (accession no. BX897699). The ST containing this allele was designated as ST-15. Phylogenetic tree analysis revealed that ST-15 belongs to Group 1 and is closely related to ST-1 (Fig. 1). In the MLST analysis, ST-1 was common among cat isolates, and human clinical specimens were assigned to ST-1 at a much higher frequency (100%) than that observed in previous studies (Iredell *et al.*, 2003; Lindroos *et al.*, 2006; Arvand *et al.*, 2007). However, the clonal population of ST-1 in Japan is quite different from that reported in other regions.

To generate a clearer population structure, we analyzed the 55 strains using the highly variable intergenic spacer S1. We identified eight different S1 genotypes, three of which were novel (Table 2). S1 genotype 11 containing a sixfold repetition of the 15-bp sequence was found in YC-053. S1 genotype 12 with a single nucleotide deletion at position 1 412 654 of the *B. henselae* Houston-1 (accession no. BX89 7699) was found in YC-012 and YC-013. The third novel S1 genotype was found in three cat isolates YC-015, YC-024, and YC-073, which contained atypical numbers of VNTRs in the two spacer S1 regions (Fig. 2). The complete genome sequence of *B. henselae* Houston-1 (accession no. BX897699) was shown to contain two identical copies of intergenic spacer S1. Locus-specific PCR, followed by direct sequencing revealed that these isolates were assigned to S1 genotype 7+4 (Fig. 2 and Table 3).

Compared with MLST, the intergenic spacer S1 was able to generate a clearer population structure of the strains under investigation. The 52 ST-1 strains were classified into seven distinct S1 genotypes. Our results indicate that ST-1 has a high genetic diversity on the basis of the sequence diversity of intergenic spacer S1. MLST could not clearly differentiate between strains because the eight selected

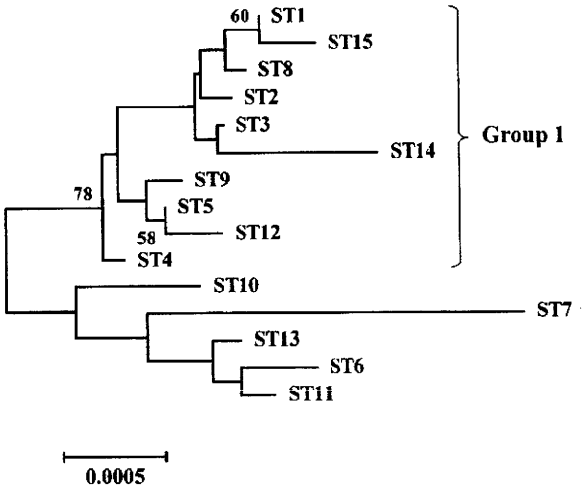


**Fig. 1.** Neighbor-joining tree of concatenated MLST allele sequences of 15 *Bartonella henselae* STs. Concatenated MLST allele sequences representing each ST were obtained for 14 previously reported STs and the new ST-15, and a neighbor-joining tree was generated by performing bootstrap analyses (1000 replicates) using MEGA4. Only node values > 50% are indicated in the figure.

**Table 1.** Multilocus sequence typing of 31 *Bartonella henselae* isolates from domestic cats

| | Allele number | | | | | | | | No. of |
|---|---|---|---|---|---|---|---|---|---|
| ST | *rrs* | *batR* | *gltA* | *ftsZ* | *groEL* | *nlpD* | *ribC* | *rpoB* | isolates (*n*) |
| 1 | 1 | 1 | 1 | 1 | 1 | 1 | 1 | 1 | 28 |
| 6 | 2 | 3 | 2 | 2 | 2 | 1 | 1 | 2 | 2* |
| 15 | 1 | 1 | 1 | 1 | 1 | 1 | 1 | 5 | 1† |

**Bartonella henselae* isolates YC-012 and YC-013.
†*Bartonella henselae* isolate YC-073.

**Table 2.** Distribution of intergenic spacer S1 genotypes among 55 human and cat *Bartonella henselae* strains

| | No. of strains (*n*) | |
|---|---|---|
| S1 genotype | Human | Cat |
| 3 | 1 | 0 |
| 4 | 12 | 14 |
| 5 | 9 | 10 |
| 7 | 1 | 1 |
| 8 | 1 | 0 |
| 11 | 0 | 1 |
| 12 | 0 | 2 |
| 7+4* | 0 | 3 |

*S1 genotype 7+4 indicates that the strain had two different copies of intergenic spacer S1 in its genome.

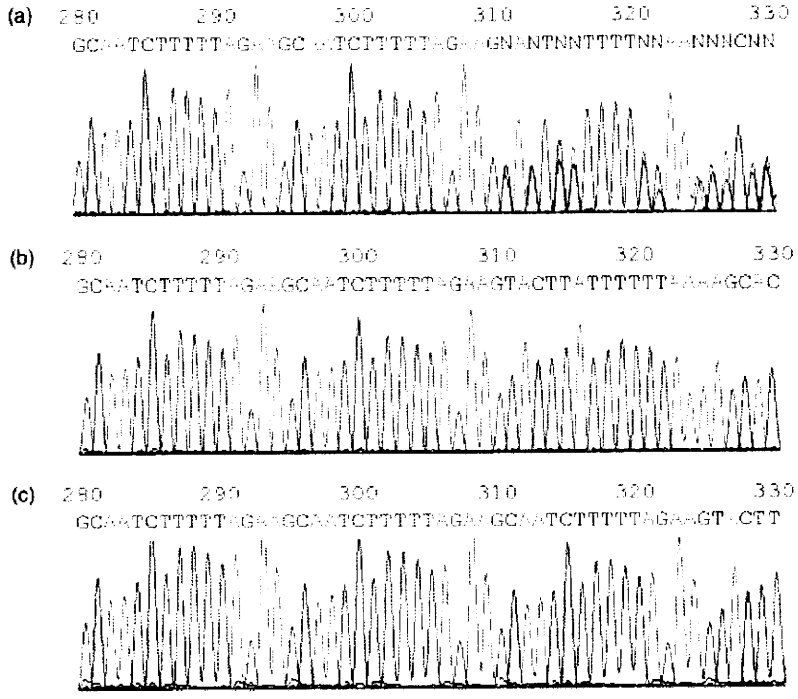


**Fig. 2.** Representative results of direct sequencing of the 16S–23S tRNA-Ala/tRNA-Ile intergenic spacer (S1) in *Bartonella henselae* strain YC-015. These sequences show the 15-bp VNTR (CAATCTTTTTAGAAG) detected with the S1 forward primer. (a) The sequence, obtained from PCR using the S1 forward and reverse primers, shows the abrupt onset of ambiguous bases suggestive of overlapping sequences. (b) The sequence corresponding to the 1 412 349–1 412 683 position of BX897699, obtained from PCR using the S1 forward and BH12700-R primers, shows a double repetition of the 15-bp VNTR and belongs to S1 genotype 7. (c) The sequence corresponding to the 1 582 358–1 582 692 position of BX897699, obtained from PCR using the S1 forward and BH13810-R primers, shows a triple repetition of the 15-bp VNTR and belongs to S1 genotype 4. The same results were obtained from *B. henselae* strains YC-024 and YC-073.

**Table 3.** Profiles of S1 genotype at two different positions in the YC-015, YC-024, and YC-073 strains

| | Spacer position on the genome* | |
|---|---|---|
| | 1 412 349–1 412 683 | 1 582 358–1 582 692 |
| S1 genotype | 7 | 4 |
| No. of 15-bp repeat | 2 | 3 |

**Bartonella henselae* Houston-1 (accession no. BX897699).

housekeeping genes were highly conserved and showed less sequence variability.

According to the intergenic spacer S1 sequence, two major S1 genotypes, 4 and 5, were identified in both human and cat strains (Table 2). In a previous MST study of *B. henselae* specimens isolated from patients in France, only S1 genotypes 3 (53.3%) and 5 (45.3%) were observed (Li *et al.*, 2007). S1 genotype 3 was not a predominant genotype in our study, and S1 genotype 4 was not detected in France. This discrepancy may be explained by similar regional differences observed in the distribution of S1 genotypes 3 and 4 among cats in France (Li *et al.*, 2006) and Japan, respectively. These data suggest that prevalent S1 genotypes among cats are often involved in human infections. Further studies are necessary to elucidate the association of the S1 genotype with pathogenicity.

In conclusion, we have demonstrated that the predominant *B. henselae* MLST in Japan, ST-1, is a significantly genetically diverse population on the basis of the sequence diversity of intergenic spacer S1, and that highly prevalent S1 genotypes among cats are often involved in human infections. These results may aid our understanding of the population structure and the relationship between human and cat strains of *B. henselae*.

## Acknowledgements

This work was supported by Grant-in-Aid for Young Scientists (B) No. 21790538 from the Ministry of Education, Culture, Sports, Science and Technology of Japan.

## References

Anderson B, Sims K, Regnery R, Robinson L, Schmidt MJ, Goral S, Hager C & Edwards K (1994) Detection of *Rochalimaea henselae* DNA in specimens from cat scratch disease patients by PCR. *J Clin Microbiol* **32**: 942–948.

Anderson BE & Neuman MA (1997) *Bartonella* spp. as emerging human pathogens. *Clin Microbiol Rev* **10**: 203–219.

Arvand M, Feil EJ, Giladi M, Boulouis HJ & Viezens J (2007) Multi-locus sequence typing of *Bartonella henselae* isolates from three continents reveals hypervirulent and feline-associated clones. *PLoS One* **2**: e1346.

Bergmans AM, Schellekens JF, van Embden JD & Schouls LM (1996) Predominance of two *Bartonella henselae* variants

among cat-scratch disease patients in the Netherlands. *J Clin Microbiol* **34**: 254–260.

Boulouis HJ, Chang CC, Henn JB, Kasten RW & Chomel BB (2005) Factors associated with the rapid emergence of zoonotic *Bartonella* infections. *Vet Res* **36**: 383–410.

Drancourt M, Birtles R, Chaumentin G, Vandenesch F, Etienne J & Raoult D (1996) New serotype of *Bartonella henselae* in endocarditis and cat-scratch disease. *Lancet* **347**: 441–443.

Iredell J, Blanckenberg D, Arvand M, Grauling S, Feil EJ & Birtles RJ (2003) Characterization of the natural population of *Bartonella henselae* by multilocus sequence typing. *J Clin Microbiol* **41**: 5071–5079.

Jensen WA, Fall MZ, Rooney J, Kordick DL & Breitschwerdt EB (2000) Rapid identification and differentiation of *Bartonella* species using a single-step PCR assay. *J Clin Microbiol* **38**: 1717–1722.

Kordick DL, Wilson KH, Sexton DJ, Hadfield TL, Berkhoff HA & Breitschwerdt EB (1995) Prolonged *Bartonella* bacteremia in cats associated with cat-scratch disease patients. *J Clin Microbiol* **33**: 3245–3251.

La Scola B & Raoult D (1999) Culture of *Bartonella quintana* and *Bartonella henselae* from human samples: a 5-year experience (1993 to 1998). *J Clin Microbiol* **37**: 1899–1905.

La Scola B, Liang Z, Zeaiter Z, Houpikian P, Grimont PA & Raoult D (2002) Genotypic characteristics of two serotypes of *Bartonella henselae*. *J Clin Microbiol* **40**: 2002–2008.

Li W, Chomel BB, Maruyama S, Guptil L, Sander A, Raoult D & Fournier PE (2006) Multispacer typing to study the genotypic distribution of *Bartonella henselae* populations. *J Clin Microbiol* **44**: 2499–2506.

Li W, Raoult D & Fournier PE (2007) Genetic diversity of *Bartonella henselae* in human infection detected with multispacer typing. *Emerg Infect Dis* **13**: 1178–1183.

Li W, Raoult D & Fournier PE (2009) Bacterial strain typing in the genomic era. *FEMS Microbiol Rev* **33**: 892–916.

Lindroos H, Vinnere O, Mira A, Repsilber D, Naslund K & Andersson SG (2006) Genome rearrangements, deletions, and amplifications in the natural population of *Bartonella henselae*. *J Bacteriol* **188**: 7426–7439.

Maiden MC (2000) High-throughput sequencing in the population analysis of bacterial pathogens of humans. *Int J Med Microbiol* **290**: 183–190.

Maruyama S, Nakamura Y, Kabeya H, Tanaka S, Sakai T & Katsube Y (2000) Prevalence of *Bartonella henselae*, *Bartonella clarridgeiae* and the 16S rRNA gene types of *Bartonella henselae* among pet cats in Japan. *J Vet Med Sci* **62**: 273–279.

Murakami K, Tsukahara M, Tsuneoka H, Iino H, Ishida C, Tsujino K, Umeda A, Furuya T, Kawauchi S & Sasaki K (2002) Cat scratch disease: analysis of 130 seropositive cases. *J Infect Chemother* **8**: 349–352.

Regnery RL, Olson JG, Perkins BA & Bibb W (1992) Serological response to "*Rochalimaea henselae*" antigen in suspected cat-scratch disease. *Lancet* **339**: 1443–1445.

Rodrick D, Dillon B, Dexter M, Nicholson I, Marcel S, Dickeson D & Iredell J (2004) Culture-negative endocarditis due to Houston complex *Bartonella henselae* acquired in Noumea, New Caledonia. *J Clin Microbiol* **42**: 1846–1848.

Tamura K, Dudley J, Nei M & Kumar S (2007) MEGA4: Molecular Evolutionary Genetics Analysis (MEGA) software version 4.0. *Mol Biol Evol* **24**: 1596–1599.

Tsuneoka H & Tsukahara M (2006) Analysis of data in 30 patients with cat scratch disease without lymphadenopathy. *J Infect Chemother* **12**: 224–226.

Tsuneoka H, Ishida C, Umeda A, Inokuma H & Tsukahara M (2004) Evaluation of isolation media for the detection of *Bartonella henselae* – isolation of *Bartonella henselae* from domestic cats. *Kansenshogaku Zasshi* **78**: 574–579.

Welch DF, Pickett DA, Slater LN, Steigerwalt AG & Brenner DJ (1992) *Rochalimaea henselae* sp. nov., a cause of septicemia, bacillary angiomatosis, and parenchymal bacillary peliosis. *J Clin Microbiol* **30**: 275–280.

Woestyn S, Olive N, Bigaignon G, Avesani V & Delmee M (2004) Study of genotypes and *virB4* secretion gene of *Bartonella henselae* strains from patients with clinically defined cat scratch disease. *J Clin Microbiol* **42**: 1420–1427.

Liver INTERNATIONAL
OFFICIAL JOURNAL OF THE INTERNATIONAL ASSOCIATION FOR THE STUDY OF THE LIVER

Liver International ISSN 1478-3223

BASIC STUDIES

# A glycyrrhizin-containing preparation reduces hepatic steatosis induced by hepatitis C virus protein and iron in mice

Masaaki Korenaga[1], Isao Hidaka[2], Sohji Nishina[1], Aya Sakai[3], Akane Shinozaki[3], Toshikazu Gondo[4], Takakazu Furutani[5], Hiroo Kawano[6], Isao Sakaida[2] and Keisuke Hino[1]

1 Department of Hepatology and Pancreatology, Kawasaki Medical University, Okayama, Japan
2 Department of Gastroenterology and Hepatology, Yamaguchi University Graduate School of Medicine, Yamaguchi, Japan
3 Department of Basic Laboratory Sciences, Yamaguchi University Graduate School of Medicine, Yamaguchi, Japan
4 Department of Surgical Pathology, Yamaguchi University Hospital, Yamaguchi, Japan
5 Department of Gastroenterology and Hepatology, Shuto General Hospital, Yamaguchi, Japan
6 Department of Pathology, Yamaguchi University Graduate School of Medicine, Yamaguchi, Japan

**Keywords**
carnitine palmitoyl transferase – mitochondria – oxidative stress – reactive oxygen species – transgenic mice

**Abbreviations**
ALT, alanine aminotransferase; ATF6, activating transcription factor 6; $CCl_4$, carbon tetrachloride; CHOP, CCAAT/enhancer-binding protein homology protein; CPT, carnitine palmitoyl transferase; ER, endoplasmic reticulum; FAS, fatty acid synthetase; γ-GCS, γ-glutamylcysteine synthetase; GSH, reduced glutathione; HCC, hepatocellular carcinoma; HCV, hepatitis C virus; IRE1, inositol-requiring enzyme 1; NAC, *N*-acetyl cysteine; PERK, PKR-like ER kinase; p-eIF2α, phosphorylated eukaryotic initiation factor-2α; PKR, RNA-activated protein kinase; ROS, reactive oxygen species; RT-PCR, reverse-transcription polymerase chain reaction; SNMC, Stronger Neo-Minophagen C; SREBP1, sterol regulatory element-binding protein 1; XBP-1, X-box DNA-binding protein 1.

**Correspondence**
Keisuke Hino, MD, PhD, Department of Hepatology and Pancreatology, Kawasaki Medical University, 577 Matsushima, Kurashiki, Okayama 701-0192, Japan
Tel: +81-86-4621111
Fax: +81-86-4641196
e-mail: khino@med.kawasaki-m.ac.jp

Received 1 July 2010
Accepted 7 January 2011

DOI:10.1111/j.1478-3231.2011.02469.x

## Abstract

*Background/Aim:* A European randomized trial showed biochemical effects of 6-month treatment with Stronger Neo-Minophagen C™ (SNMC), a glycyrrhizin-containing preparation, in patients with chronic hepatitis C, but its underlying mechanisms remain elusive. We reported previously that SNMC exhibits an anti-oxidative effect in hepatitis C virus (HCV) transgenic mice that develop marked hepatic steatosis with mitochondrial injury under iron overloading. Hepatic steatosis and iron overload are oxidative stress-associated pathophysiological features in chronic hepatitis C. The aim of this study was to investigate whether long-term treatment with SNMC could prevent the development of hepatic steatosis in iron-overloaded HCV transgenic mice. *Methods:* C57BL/6 transgenic mice expressing the HCV polyprotein were fed an excess iron diet concomitantly with intraperitoneal injection of saline, SNMC, or seven-fold-concentrated SNMC thrice weekly for 6 months. *Results:* Stronger Neo-Minophagen C™ inhibited the development of hepatic steatosis in a dose-dependent manner without affecting hepatic iron content, attenuated ultrastructural alterations of mitochondria of the liver, activated mitochondrial β-oxidation with increased expression of carnitine palmitoyl transferase I and decreased the production of reactive oxygen species in the liver in iron-overloaded transgenic mice. However, SNMC hardly affected the unfolded protein response, which post-transcriptionally activates sterol regulatory element-binding protein 1, a transcription factor involved in lipid synthesis, even though we reported previously the activation of the unfolded protein response in the same iron-overloaded transgenic mice. *Conclusions:* These results suggest that SNMC prevents hepatic steatosis possibly by protecting mitochondria against oxidative stress induced by HCV proteins and iron overload.

Hepatitis C virus (HCV) causes acute and chronic hepatitis, cirrhosis and hepatocellular carcinoma (HCC) (1). Because current antiviral treatment can only eliminate the virus in approximately 50% of patients (2), therapies to reduce disease progression in chronically infected individuals would be of great benefit. In Japan, Stronger Neo-Minophagen C™ (SNMC), a glycyrrhizin-containing preparation, has been used as a treatment for

chronic hepatitis for more than 30 years. SNMC contained glycyrrhizin as the main active ingredient at first, and later a change was made in its composition on the basis of pharmacological studies including animal experiments and clinical studies. Currently, it is available in an injectable form for intravenous administration, containing 0.2% glycyrrhizin, 0.1% L-cystein and 2.0% glycine in physiological solution. A recent European randomized trial showed biochemical effects of 26-week treatment with SNMC in patients with chronic hepatitis C (3). In addition, Arase *et al.* (4) demonstrated that long-term usage of SNMC was effective in preventing HCC development in Japanese patients with chronic hepatitis C. However, the mechanisms by which SNMC prevents disease progression of chronic hepatitis C remain elusive.

Oxidative stress has been proposed to be one of the mechanisms of liver injury in HCV-associated chronic liver diseases (5), and hepatic steatosis and/or mitochondrial injury are well-known features in chronic hepatitis C (6, 7). We reported that HCV transgenic mice fed an excess iron diet show marked steatosis and mitochondrial injury at 6 months, and an increase in the hepatic lipid peroxidation products and the subsequent development of HCC at 12 months after the initiation of feeding (8). We also showed that a single injection of SNMC protected hepatocytes against carbon tetrachloride ($CCl_4$)-induced oxidative stress and mitochondrial injury in these transgenic mice without iron overload (9). These results prompted us to investigate whether SNMC inhibited the development of hepatic steatosis in terms of prevention of disease progression in chronic hepatitis C. The aim of this study was to examine whether long-term treatment with SNMC could prevent the development of hepatic steatosis in HCV transgenic mice fed an excess iron diet. In the present study, we show that SNMC reduces hepatic steatosis induced by HCV protein and iron overload in mice by means of a protective effect against mitochondrial injury.

## Materials and methods

### Animals and experimental design

The transgene pAlbSVPA-HCV, containing the full-length polyprotein-coding region under the control of the murine albumin promoter/enhancer, was described in detail (10, 11). Of the four transgenic lineages with evidence of RNA transcription of the full-length HCV-N open reading frame (FL-N), the FL-N/35 lineage proved capable of breeding in large numbers. There is no inflammation in the transgenic liver (11). Male FL-N/35 transgenic mice were fed an excess iron diet (carbonyl iron 225 mg/kg diet) at the age of 8 weeks, injected intraperitoneally with 50 µl of saline (control), SNMC or seven-fold-concentrated SNMC (supplied by Minophagen Pharmaceutical Co. Ltd, Tokyo, Japan) three times weekly and killed by intraperitoneal injection of 10% pentbarbital sodium preceded by 12-h fasting at 6 months after initiation of feeding according to the criteria outlined in the Guide for the Care and Use of Laboratory Animals.

### Histological procedures

A portion of liver tissue was immediately snap frozen in liquid nitrogen for RNA extraction, protein extraction and determination of hepatic triglyceride and iron concentrations. The remaining liver tissue was fixed in 4% paraformaldehyde in phosphate-buffered saline and embedded in paraffin for histological analysis. Liver sections were stained with haematoxylin and eosin and Masson's trichrome method for fibrosis.

### Hepatic triglyceride content

Lipids were extracted from the homogenized liver tissue by the method of Bligh and Dyer (12). The triglyceride levels were measured with a TGE test Wako kit (Wako Pure Chemicals, Tokyo, Japan), according to the manufacturer's instructions. Protein concentrations in liver were determined by the method of Lowry *et al.* (13), using a DC protein assay kit (Bio-Rad Laboratories, Hercules, CA, USA).

### Hepatic iron concentration and hepcidin mRNA

The iron concentration in the liver was measured by atomic absorption spectrometry (Hitachi Z-6100, Tokyo, Japan), as described previously (8), and expressed as micrograms Fe/g of tissue (wet weight). One-step real-time reverse-transcription polymerase chain reaction was also performed as described previously (8). The primers amplifying the genes coding hepcidin and β-actin were as follows: hepcidin, sense; TCCTGCTTCTCCTCCTTGCC, antisense; GTCTGCCCTGCTTTCTTCCC (GenBank accession number, NM_032541) and β-actin, sense; TGACAGGATGCAGAAGGAGA, antisense; GCTGGAA GGTGGACAGTGAG (GenBank accession number, NM_ 007393).

### Immunoblotting

Lysates of liver were separated by sodium dodecyl sulphate–polyacrylamide gel electrophoresis. The proteins were transferred to polyvinylidene difluoride membranes (Millipore, Bedford, MA, USA), blocked overnight at 4 °C with 5% skim milk and 0.1% Tween 20 in Tris-buffered saline, and subsequently incubated for 1 h at room temperature with an anti-rabbit carnitine palmitoyl transferase I (CPTI) antibody, anti-rabbit CPTII antibody (Alpha Diagnostic International, San Antonio, TX, USA), anti-rabbit sterol regulatory element-binding protein 1 (SREBP1) antibody (Santa Cruz Biotechnology Inc., Santa Cruz, CA, USA), anti-rabbit fatty acid synthetase (FAS) antibody (Cell Signaling Technology Inc., Boston, MA, USA), anti-mouse X-box

DNA-binding protein 1 (XBP-1) antibody (Santa Cruz Biotechnology Inc.) or anti-bacterially expressed, mouse CCAAT/enhancer-binding protein homology protein (CHOP) fusion protein antibody (Abcam, Cambridge, UK). Exceptionally, the proteins were blocked for 1 h at room temperature and subsequently incubated overnight at 4 °C with an anti-rabbit phosphorylated eukaryotic initiation factor-2α (p-eIF2α) antibody (Cell Signaling Technology Inc.).

### Electron microscopy

Liver specimens were fixed in 2.1% glutaraldehyde, post-fixed in 1% osmium tetroxide, dehydrated in graded ethanol and propylene dioxide and embedded in Epok. Thick sections (1 μm in width) were stained with toluidine blue to identify steatosis by light microscopy. Thin sections were stained with uranyl acetate and lead citrate, and examined using a Hitachi-7000 transmission electron microscope (Hitachi Ltd., Tokyo, Japan). The length of mitochondria was measured using IMAGE-PRO PLUS 4.0 software (Media Cybernetics Inc., Bethesda, MD, USA) for two randomly selected areas of electron microscopic images in each mice to quantify ultrastructural alterations of mitochondria.

### *In vivo* formation of [$^{14}$C]$CO_2$ from [U-$^{14}$C] palmitic acid

A tracer dose of [U-$^{14}$C] palmitic acid (150 μCi/kg; 0.16 μmol/kg, American Biosciences, St Louis, MO, USA) was administered by gastric intubation in 0.2 ml of corn oil, preceded by fasting for 42 h, as described previously (8). The animal was then placed for 6 h in a small plastic cage swept by an airflow of 50 ml/min. The outflow was bubbled into 30 ml of monoethanolamine. After 6 h, 1 ml was removed and counted for [$^{14}$C] $CO_2$ activity with an Aloka Liquid Scintillation Counter 5100 (Aloka Co. Ltd., Tokyo, Japan).

### *In situ* detection of reactive oxygen species

*In situ* reactive oxygen species (ROS) production in the liver was assessed by staining with dihydroethidium as described previously (14). In the presence of ROS, dihydroethidium (Invitrogen Corp., Carlsbad, CA, USA) is oxidized to ethidium bromide and stains nuclei bright red by intercalating with the DNA (15). Fluorescence intensity was quantified using NIH image analysis software for three randomly selected areas of digital images for each mouse.

### Statistical analysis

Quantitative values are expressed as mean ± SD. Two groups among multiple groups were compared by the rank-based, Kruskal–Wallis ANOVA test followed by the Scheffé test. Data between two groups were compared by Student's *t*-test. A $P$ value of $< 0.05$ was considered to be significant.

## Results

### Serum alanine aminotransferase levels and hepatic triglyceride accumulation

Six-month treatment with SNMC or seven-fold-concentrated SNMC significantly reduced serum alanine aminotransferase (ALT) ($P < 0.05$) in FL-N/35 transgenic mice fed the excess iron diet (Fig. 1A). Transgenic mice fed the excess iron diet developed severe steatosis including the centrilobular microvesicular type, as described previously (8, 16). SNMC reduced hepatic triglyceride content in a dose-dependent manner ($P < 0.05$, $P < 0.01$, Fig. 1B). SNMC obviously reduced the centrilobular microvesicular steatosis and moderately decreased hepatic steatosis in the remaining areas of hepatic lobules, whereas seven-fold-concentrated SNMC almost completely suppressed hepatic steatosis (Fig. 1C). Mice in the three groups (control, SNMC and seven-fold-concentrated SNMC) showed no evidence of intrahepatic inflammation or fibrosis.

### Hepatic iron content

We reported that iron overload reinforced hepatic steatosis in FL-N/35 transgenic mice (8). We first measured hepatic iron levels and the expression of hepcidin, a negative regulator in iron homeostasis, to assess whether SNMC attenuated hepatic iron overload. As shown in Figure 2, 6-month treatment with SNMC or seven-fold-concentrated SNMC changed neither the hepatic iron level nor the hepcidin expression in transgenic mice fed the excess iron diet, suggesting that SNMC inhibited hepatic steatosis without affecting iron overload.

### Mitochondrial ultrastructure

As we observed previously the attenuation of $CCl_4$-induced ultrastructural alterations of mitochondria by SNMC in FL-N/35 transgenic mice (9), and found obvious reduction of centrilobular microvesicular steatosis by SNMC in the present study, we next examined the ultrastructure of the hepatic mitochondria in FL-N/35 transgenic mice fed the excess iron diet. Ultrastructural alterations such as irregularly sized mitochondria, swollen mitochondria or disorganized cristae that were observed in FL-N/35 transgenic mice fed the excess iron were much less frequently found after the 6-month treatment with SNMC in a dose-dependent manner (Fig. 3A–C). The mean length of mitochondria was significantly greater in mice without SNMC than in those with SNMC (Fig. 3D). Thus, SNMC attenuated ultrastructural alterations of mitochondria of the liver in FL-N/35 transgenic mice fed the excess iron diet.

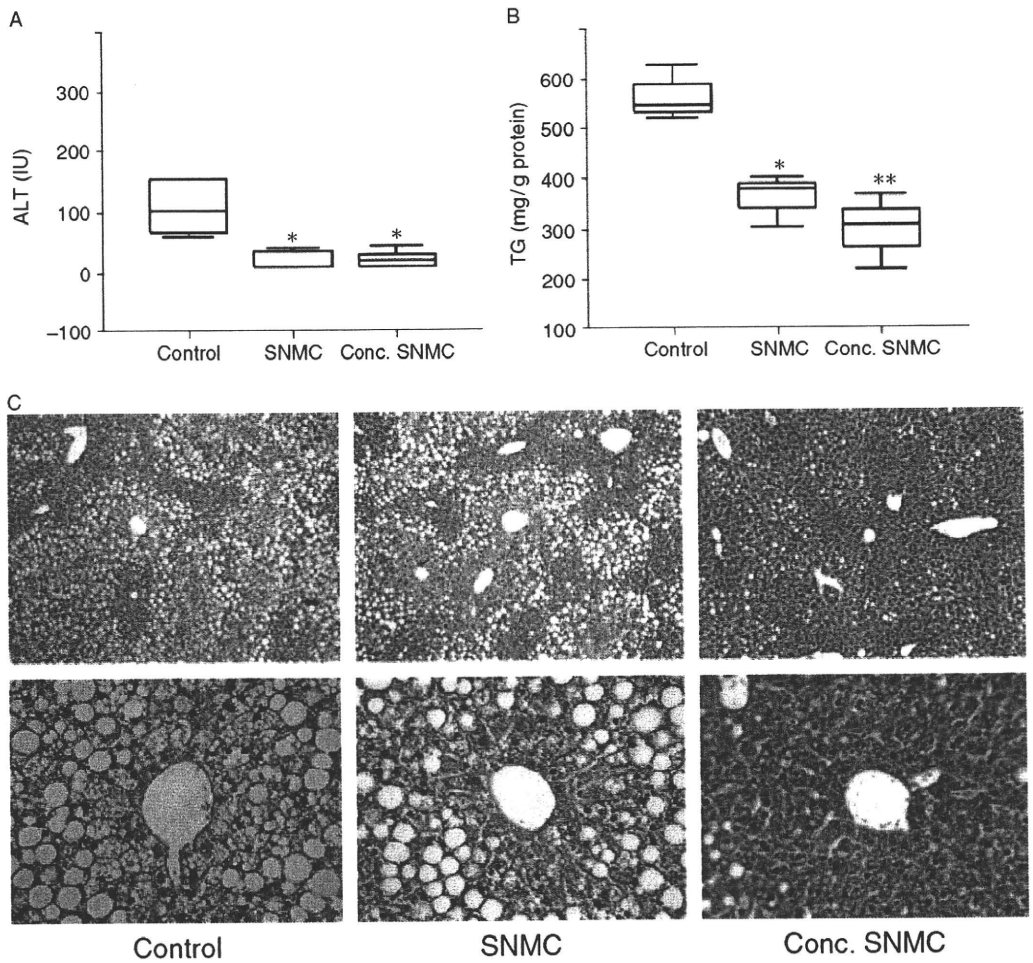


**Fig. 1.** Serum alanine aminotransferase (ALT) levels, hepatic triglyceride levels and hepatic steatosis in iron-overloaded FL-N/35 transgenic mice in three groups. (A) Serum ALT levels in six mice in each group. (B) Hepatic triglyceride levels in three mice in each group. ALT and triglyceride levels are shown as box plot profiles. The bottom and top edges of the boxes are the 25th and 75th percentiles respectively. The median value is shown by the line within the box. (C) Hepatic steatosis in mice in each group (haematoxylin and eosin, original magnification × 100 for upper panel and × 400 for lower panel). Control, transgenic mice injected intraperitoneally with 50 μl of saline three times weekly for 6 months; Stronger Neo-Minophagen C™ (SNMC), transgenic mice injected intraperitoneally with 50 μl of SNMC three times weekly for 6 months; Conc. SNMC, transgenic mice injected intraperitoneally with 50 μl of seven-fold-concentrated SNMC three times weekly for 6 months. $^{*}P < 0.05$, $P < 0.01$ vs control.

### Degradation activity of fatty acid

We next examined *in vivo* formation of $[^{14}C]CO_2$ from [U-$^{14}$C] palmitic acid (C16:0) to assess whether SNMC improved mitochondrial function. Palmitic acid is a long-chain fatty acid. Mitochondria catalyse the β-oxidation of the bulk of short-, medium- and long-chain fatty acids (17). As shown in Figure 4A, SNMC significantly increased the *in vivo* formation of $[^{14}C]CO_2$ from [U-$^{14}$C] palmitic acid in FL-N/35 transgenic mice fed the excess iron diet ($P < 0.05$). These results suggested that SNMC improved mitochondrial β-oxidation activity.

### Carnitine palmitoyl transferase I expression

Carnitine palmitoyl transferase I and CPTII regulate oxidation of long-chain fatty acids in the mitochondria. CPTI, a transmembrane enzyme of the mitochondrial outer membrane, has been shown to be the rate-limiting step in the β-oxidation of long-chain fatty acids (18). The expression of CPTI, but not CPTII, significantly increased after the 6-month treatment with SNMC or seven-fold-concentrated SNMC ($P < 0.005$, Fig. 4B). We reported previously the decreased expression of CPTI in FL-N/35 transgenic mice fed the excess iron diet as compared with nontransgenic mice fed the control diet

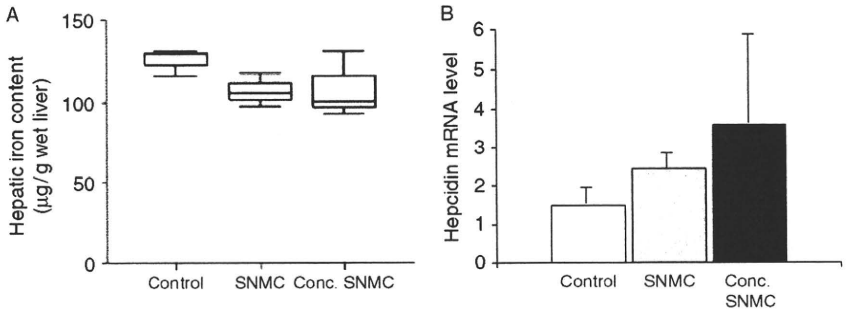


**Fig. 2.** Iron content and hepcidin mRNA expression in the liver in iron-overloaded FL-N/35 transgenic mice in each group. (A) Hepatic iron concentrations were measured by atomic absorption spectrometry in three mice in each group. The results are shown as box plot profiles. The bottom and top edges of the boxes are the 25th and 75th percentiles respectively. The median value is shown by the line within the box. (B) The expression levels of hepcidin mRNA was measured by reverse-transcription polymerase chain reaction in three mice in each group. The relative quantities of hepcidin mRNA were normalized to β-actin mRNA. Control, Stronger Neo-Minophagen C™ (SNMC) and Conc. SNMC; see legend for Figure 1.

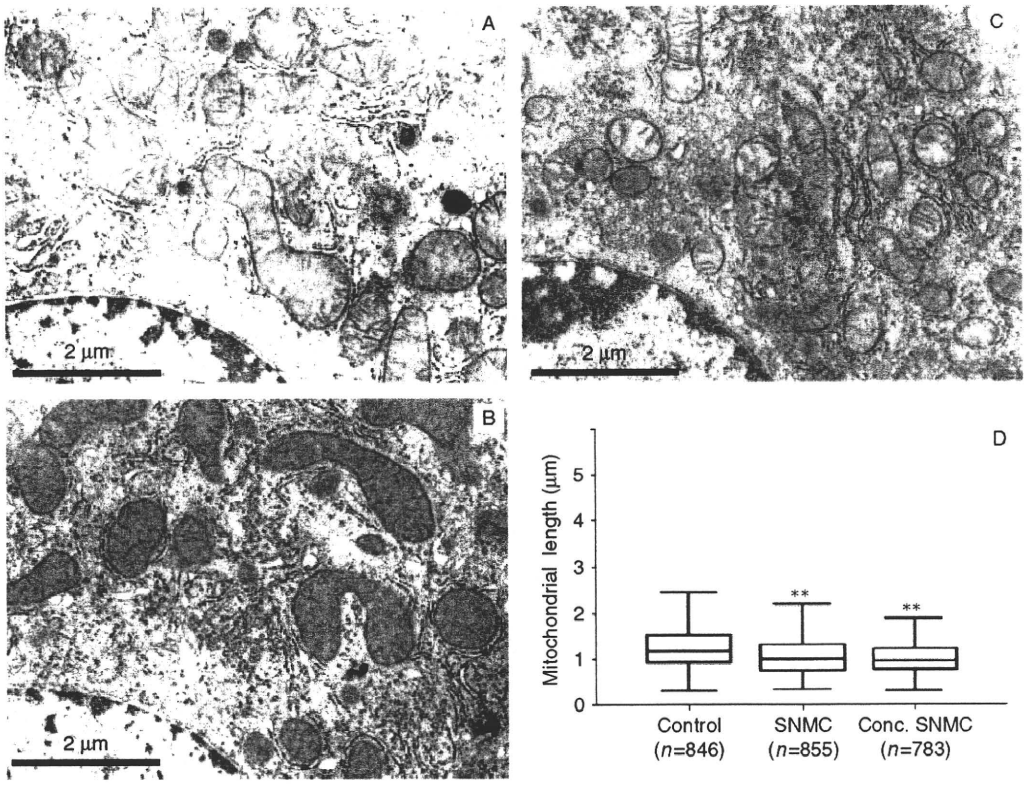


**Fig. 3.** Electron microscopy of the liver of an iron-overloaded FL-N/35 transgenic mouse from each group. Ultrastructural alterations such as irregularly sized mitochondria, swollen mitochondria and disorganized cristae that were observed in the iron-overloaded FL-N/35 transgenic mouse were much less frequently found after a 6-month treatment with Stronger Neo-Minophagen C™ (SNMC) in a dose-dependent manner. The magnification scale is indicated in the left-lower corner of each picture. The length of mitochondria was assessed for three mice in each group and measured using IMAGE-PRO PLUS 4.0 software for two randomly selected areas of electron microscopic images in each mice. The numbers in parentheses represent the total number of mitochondria examined in each group. Control, SNMC and Conc. SNMC; see legend for Figure 1. (A) Control; (B) SNMC; (C) Conc. SNMC; and (D) the length of mitochondria. $^{**}P < 0.0001$ vs control.

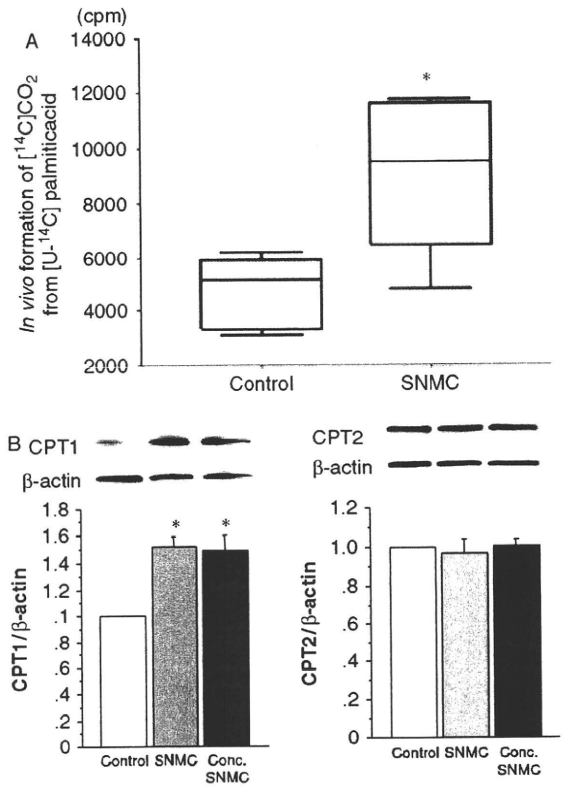


**Fig. 4.** *In vivo* formation of [$^{14}$C]$CO_2$ from [U-$^{14}$C] palmitic acid and hepatic expression of carnitine palmitoyl transferase I (CPTI) and CPTII in iron-overloaded FL-N/35 transgenic mice in each group. (A) A tracer dose of [U-$^{14}$C] palmitic acid (150 μCi/kg; 0.16 μmol/kg) was administered by gastric intubation in 0.2 ml of corn oil, preceded by fasting for 42 h. The animal was then placed for 6 h in a small plastic cage swept by an airflow of 50 ml/min. The outflow was bubbled into 30 ml of monoethanolamine. After 6 h, 1 ml was removed and counted for [$^{14}$C] $CO_2$ activity. This experiment was carried out for five mice in each group. The results are shown as box plot profiles. The bottom and top edges of the boxes are the 25th and 75th percentiles respectively. The median value is shown by the line within the box. (B) Immunoblots for CPTI and CPTII were performed using liver lysates from four mice in each group. The degree of protein expression was normalized with β-actin. Control, Stronger Neo-Minophagen C™ (SNMC) and Conc. SNMC; see legend for Figure 1. *$P < 0.05$ vs control.

(16), which may be related to the association of HCV core protein with the mitochondrial outer membrane (19). Together with improvement of the mitochondrial structure, β-oxidation activity and CPTI expression, SNMC had a protective effect against mitochondrial injury induced by HCV proteins and iron overload.

### Reactive oxygen species production

We have reported previously that HCV core protein increases ROS production through inhibition of mitochondrial electron transport (19), and found increased ROS production in FL-N/35 transgenic mice fed the excess iron diet as compared with nontransgenic mice fed the control diet (16). Therefore, we evaluated *in situ* ROS production to assess whether SNMC reduces ROS production in the liver in terms of a protective effect against mitochondrial injury. ROS production was significantly reduced by SNMC in a dose-dependent manner ($P < 0.005$, $P < 0.001$, Fig. 5). Thus, SNMC reduced hepatic steatosis by protecting mitochondria against oxidative stress induced by HCV proteins and iron overload.

### Unfolded protein response and sterol regulatory element-binding protein 1 expression

We next evaluated the effect of SNMC on the unfolded protein response and the expression of SREBP1, a transcription factor that activates genes required for lipogenesis (20), because we found in our previous study that not only the decreased CPTI expression but also the increased SREBP1 expression owing to the activated unfolded protein response contributed to the development of hepatic steatosis in FL-N/35 transgenic mice fed the excess iron diet (16). The unfolded protein response signalling cascades are initiated by three endoplasmic reticulum (ER)-resident sensors: inositol-requiring enzyme 1 (IRE1), RNA-activated protein kinase-like ER kinase (PERK) and activating transcription factor 6 (ATF6) (21). IRE1 activation splices unspliced XBP-1 (uXBP-1) to form spliced XBP-1 (sXBP-1) mRNA (22), and was assessed by the sXBP-1 protein level (23). PERK activation was evaluated by measurement of p-eIF2α and CHOP (24). ATF6 activation was assessed by uXBP-1 expression (25). Six-month treatment with SNMC or seven-fold-concentrated SNMC did not change the expression of sXBP-1, CHOP, SREBP1 or FAS, a target gene of SREBP1, but decreased the expression of uXBP-1 and p-eIF2α (Fig. 6). These results suggested that SNMC inhibited hepatic steatosis through a protective effect against mitochondrial injury rather than restoration of activated lipogenesis in FL-N/35 transgenic mice fed the excess iron diet, even though it may attenuate the unfolded protein response to some degree.

## Discussion

Hepatic steatosis and iron overload are not only pathophysiological features of HCV-associated chronic liver disease (5, 26) but also risk factors for the development of HCC (27, 28). The present animal model, FL-N/35 transgenic mice fed an excess iron diet, had several similarities with patients having HCV-associated chronic liver disease in terms of development of hepatic steatosis, followed by hepatocarcinogenesis (8), even though hepatic steatosis in this model was different from one observed in patients with HCV genotype 3 infection as to whether it was virally induced. In addition, the hepatic

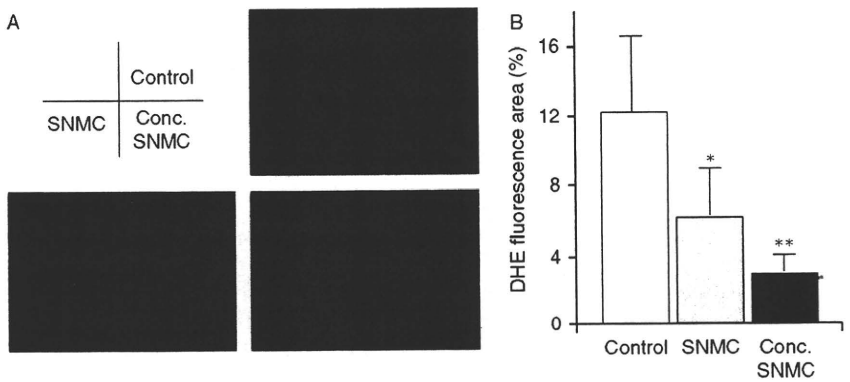


**Fig. 5.** Reactive oxygen species production in the liver in iron-overloaded FL-N/35 transgenic mice in each group. (A) Frozen liver sections of mice in each group were stained with dihydroethidium. (B) Fluorescence intensity was quantified by NIH image analysis software for three randomly selected areas of digital images for four mice in each group. Control, Stronger Neo-Minophagen C$^{TM}$ (SNMC) and Conc. SNMC; see legend for Figure 1. $^{*}P < 0.005$ vs control, $^{**}P < 0.001$ vs control, $P < 0.05$ vs SNMC.

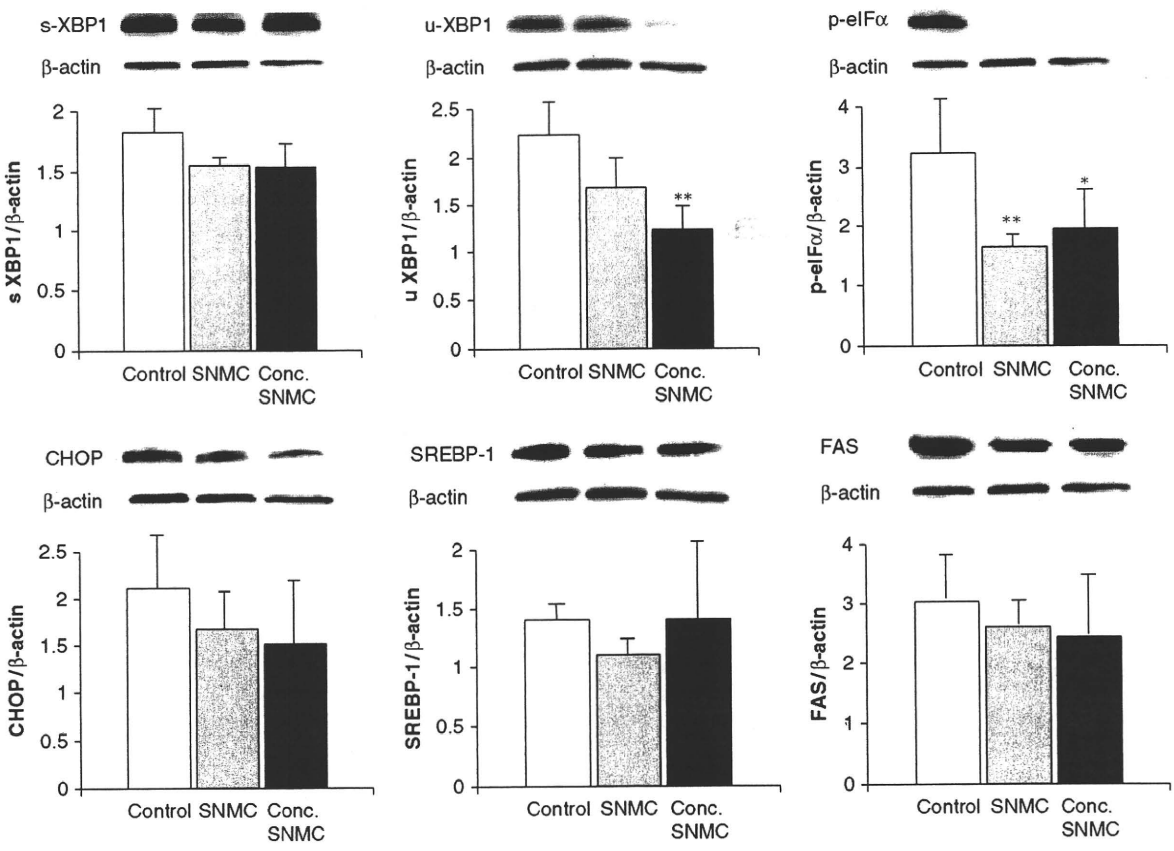


**Fig. 6.** Expression of spliced X-box DNA-binding protein 1 (sXBP-1), unspliced X-box DNA-binding protein 1 (uXBP-1), phosphorylated initiation factor-2α (p-IF2α), CCAAT/enhancer-binding protein homology protein (CHOP), sterol regulatory element-binding protein 1 (SREBP1) and fatty acid synthetase (FAS) in the liver in mice in each group. Immunoblots were performed using liver lysates from four mice in each group. The degree of protein expression was normalized with β-actin. Control, Stronger Neo-Minophagen C$^{TM}$ (SNMC) and Conc. SNMC; see legend for Figure 1. $^{*}P < 0.05$ vs control, $^{**}P < 0.01$ vs control, $P < 0.05$ vs SNMC.

iron concentration of FL-N/35 transgenic mice fed the excess iron diet was comparable with that of a large number of patients with chronic hepatitis C in extensive studies (29, 30). Thus, FL-N/35 transgenic mice fed the excess iron diet appeared to be a suitable animal model to assess the effect of the long-term treatment with SNMC on the development of hepatic steatosis in HCV infection. The dose of SNMC administered to the FL-N/35 transgenic mice was comparable with the dosage given to patients with chronic hepatitis (approximately 100 ml of SNMC). This implies that a clinical dosage of SNMC has the potential to reduce hepatic steatosis occurring in patients with HCV-associated chronic liver diseases. There was no histological improvement such as inflammation or fibrosis regardless of serum ALT reduction in the human study, where the change of hepatic steatosis was not assessed (3). We could not evaluate whether SNMC has a potential to reduce inflammation or fibrosis in this study, because the present animal model did not show inflammation or fibrosis. Therefore, the decreased serum ALT levels in this model were thought to reflect the reduction of hepatic steatosis by SNMC.

Our previous study indicated that iron overload reinforced hepatic steatosis through ROS-induced activation of the unfolded protein response in FL-N/35 transgenic mice, and that an anti-oxidant, *N*-acetyl cysteine (NAC), almost completely blocked ROS production and cancelled hepatic steatosis induced by HCV proteins and iron (16). In the present study, SNMC reduced ROS production to a lesser degree than NAC. SNMC did not affect the hepatic iron content or hepcidin expression level, even though we reported previously the ROS-associated inhibition of hepcidin transcription in FL-N/35 transgenic mice (14). Nor did SNMC fully inhibit the ROS-associated unfolded protein response; nevertheless, SNMC effectively inhibited the development of hepatic steatosis in a dose-dependent manner through improvement of the mitochondrial structure, β-oxidation activity and CPTI expression. It should be noted that SNMC had a protective effect against mitochondrial injury rather than a simple anti-oxidative effect in FL-N/35 transgenic mice fed the excess iron.

Carnitine palmitoyl transferase I is negatively regulated by malonyl-CoA, an intermediate product in fatty acid synthesis, at the transcriptional level (18). Therefore, we need to consider at least two explanations for the increased CPTI expression induced by the 6-month treatment with SNMC. HCV core protein has been shown to be located on the mitochondrial outer membrane (19, 31), which may damage the membrane. One explanation is that SNMC increases CPTI expression through the restoration of the damaged mitochondrial outer membrane, as shown by the attenuated ultrastructural alterations of mitochondria with SNMC in FL-N/35 transgenic mice fed the excess iron. Another explanation is that SNMC may increase CPTI expression through the inhibition of fatty acid synthesis. However, the latter explanation seems unlikely, because the 6-month treatment with SNMC did not change the expression of SREBP1 or FAS (Fig. 6). Thus, the mechanisms by which SNMC reduces hepatic steatosis induced by HCV protein and iron overload may be mainly because of increased β-oxidation activity associated with increased CPTI stability through the protective effect against mitochondrial injury.

Of particular concern is how SNMC exerts its protective effect against mitochondrial injury. We reported previously that SNMC restored depletion of reduced glutathione (GSH) induced by $CCl_4$ and increased the synthesis of γ-glutamylcysteine synthetase (γ-GCS), a rate-limiting enzyme regulating GSH synthesis, at the transcriptional level in FL-N/35 transgenic mice (9). Judging from the protective effect of SNMC against mitochondrial injury, SNMC may play a role in the reduction of mitochondrial oxidative stress. Hepatic GSH synthesis is mainly regulated by the availability of cysteine, the sulphur amino acid precursor and the activity of γ-GCS. SNMC consists of 0.2 glycyrrhizin, 0.1 cycteine and 2.0% glycine in physiological solution. The cysteine included in SNMC may also contribute to GSH synthesis through its increased availability. The present study was largely observational and therefore further analysis is needed to clarify the mechanisms by which SNMC exerts a protective effect against mitochondrial injury.

In conclusion, this study shows that SNMC reduces hepatic steatosis induced by HCV protein and iron overload in mice by inducing increased β-oxidation activity associated with an increased CPTI expression.

## Acknowledgements

This study was supported by a grant from the Ministry of Education, Culture, Sports, Science and Technology (No. 20590782), and in part by a Research on Hepatitis, Health and Labour Sciences Research Grants from the Ministry of Health, Labor and Welfare, Japan.

## References

1. Seeff LB. Natural history of chronic hepatitis C. *Hepatology* 2002; **36**: S35–46.
2. Fried MW, Shiffman ML, Reddy KR, *et al.* Peginterferon alfa-2a plus ribavirin for chronic hepatitis C virus infection. *N Engl J Med* 2002; **347**: 975–82.
3. Orlent H, Hansen BE, Willems M, *et al.* Biochemical and histological effects of 26 weeks of glycyrrhizin treatment in chronic hepatitis C: a randomized phase II trial. *J Hepatol* 2006; **45**: 539–46.
4. Arase Y, Ikeda K, Murashima N, *et al.* The long term efficacy of glycyrrhizin in chronic hepatitis C patients. *Cancer* 1997; **79**: 1494–500.
5. Farinati F, Cardin R, De Maria N, *et al.* Iron storage, lipid peroxidation and glutathione turnover in chronic anti-HCV positive hepatitis. *J Hepatol* 1995; **22**: 449–56.

6. Kitase A, Hino K, Furutani T, *et al.* In situ detection of oxidized n-3 polyunsaturated fatty acids in chronic hepatitis C: correlation with hepatic steatosis. *J Gastroenterol* 2005; **40**: 617–24.
7. Barbaro G, Di Lorenzo G, Asti A, *et al.* Hepatocellular mitochondrial alterations in patients with chronic hepatitis C: ultrastructural and biochemical findings. *Am J Gastroenterol* 1999; **94**: 2198–205.
8. Furutani T, Hino K, Okuda M, *et al.* Hepatic iron overload induces hepatocellular carcinoma in transgenic mice expressing the hepatitis C virus polyprotein. *Gastroenterology* 2006; **130**: 2087–98.
9. Hidaka I, Hino K, Korenaga M, *et al.* Stronger Neo-Minophagen C$^{TM}$, a glycyrrhizin-containing preparation, protects liver against carbon tetrachloride-induced oxidative stress in transgenic mice expressing the hepatitis C virus polyprotein. *Liver Int* 2007; **27**: 845–53.
10. Beard MR, Abell G, Honda M, *et al.* An infectious molecular clone of a Japanese genotype 1b hepatitis C virus. *Hepatology* 1999; **30**: 316–24.
11. Lerat H, Honda M, Beard MR, *et al.* Steatosis and liver cancer in transgenic mice expressing the structural and nonstructural proteins of hepatitis C virus. *Gastroenterology* 2002; **122**: 352–65.
12. Bligh EG, Dyer WJ. A rapid method of total lipid extraction and purification. *Can J Biochem Physiol* 1959; **37**: 911–7.
13. Lowry OH, Rosebrough NJ, Farr AL, Randall RJ. Protein measurement with the Folin phenol reagent. *J Biol Chem* 1951; **193**: 265–75.
14. Nishina S, Hino K, Korenaga M, *et al.* Hepatitis C virus-induced reactive oxygen species raise hepatic iron level in mice by reducing hepcidin transcription. *Gastroenterology* 2008; **134**: 226–38.
15. Harrison-Findik DD, Schafer D, Klein E, *et al.* Alcohol metabolism-mediated oxidative stress down-regulates hepcidin transcription and leads to increased duodenal iron transporter expression. *J Biol Chem* 2006; **281**: 22974–82.
16. Nishina S, Korenaga M, Hino K, *et al.* Hepatitis C virus protein and iron overload induce hepatic steatosis through the unfolded protein response in mice. *Liver Int* 2010; **30**: 683–92.
17. Rao MS, Reddy JK. Peroxisomal beta-oxidation and steatohepatitis. *Semin Liver Dis* 2001; **21**: 43–55.
18. Kerner J, Hoppel C. Fatty acid import into mitochondria. *Biochim Biophys Acta* 2000; **1486**: 1–17.
19. Korenaga M, Wang T, Li Y, *et al.* Hepatitis C virus core protein inhibits mitochondrial electron transport and increases reactive oxygen species (ROS) production. *J Biol Chem* 2005; **280**: 37481–8.
20. Horton JD, Goldstein JL, Brown MS. SREBPs: activators of the complete program of cholesterol and fatty acid synthesis in the liver. *J Clin Invest* 2002; **109**: 1125–31.
21. Ji C, Kaplowitz N. ER stress: can the liver cope? *J Hepatol* 2006; **45**: 321–33.
22. Calfon M, Zeng H, Urano F, *et al.* IRE1 couples endoplasmic reticulum load to secretory capacity by processing the XBP-1 mRNA. *Nature* 2002; **415**: 92–6.
23. Yoshida H, Matsui T, Yamamoto A, Okada T, Mori K. XBP1 mRNA is induced by ATF6 and spliced by IRE1 in response to ER stress to produce a highly active transcription factor. *Cell* 2001; **107**: 881–91.
24. Marciniak SJ, Ron D. Endoplasmic reticulum stress signaling in disease. *Physiol Rev* 2006; **86**: 1133–49.
25. Okada T, Yoshida H, Akazawa R, Negishi M, Mori K. Distinct roles of activating transcription factor 6 (ATF6) and double-stranded RNA-activated protein kinase-like endoplasmic reticulum kinase (PERK) in transcription during the mammalian unfolded protein response. *Biochem J* 2002; **366**: 585–94.
26. Scheuer PJ, Ashrafzadeh P, Sherlock S, Brown D, Dusheiko GM. The pathology of hepatitis C. *Hepatology* 1992; **15**: 567–71.
27. Ohata K, Hamasaki K, Toriyama K, *et al.* Hepatic steatosis is a risk factor for hepatocellular carcinoma in patients with chronic hepatitis C virus infection. *Cancer* 2003; **97**: 3036–43.
28. Kato J, Kobune M, Nakamura T, *et al.* Normalization of elevated hepatic 8-hydroxy-2′-deoxyguanosine levels in chronic hepatitis C patients by phlebotomy and low iron diet. *Cancer Res* 2001; **61**: 8697–702.
29. Hofer H, Osterreicher C, Jessner W, *et al.* Hepatic iron concentration does not predict response to standard and pegylated-IFN/ribavirin therapy in patients with chronic hepatitis C. *J Hepatol* 2004; **40**: 1018–22.
30. Rulyak SJ, Eng SC, Patel K, *et al.* Relationships between hepatic iron content and virologic response in chronic hepatitis C patients treated with interferon and ribavirin. *Am J Gastroenterol* 2005; **100**: 332–7.
31. Schwer B, Ren S, Pietschmann T, *et al.* Targeting of hepatitis C virus core protein to mitochondria through a novel C-terminal localization motif. *J Virol* 2004; **78**: 7958–68.

**Focal nodular hyperplasia-like nodule with reduced expression of organic anion transporter 1B3 in alcoholic liver cirrhosis**

Nobuko Doi[1], Yasuyuki Tomiyama[1], Tomoya Kawase [1], Sohji Nishina[1], Naoko Yoshioka[1], Yuichi Hara[1], Koji Yoshida[1], Keiko Korenaga[1], Masaaki Korenaga[1], Takuya Moriya[2], Atsushi Urakami[3], Osamu Nakashima[4], Masamichi Kojiro[4], Keisuke Hino[1]

Departments of Hepatology and Pancreatology[1], Pathology [2], and Digestive Surgery[3], Kawasaki Medical University, Kurashiki, Department of Pathology[4], Kurume University School of Medicine, Kurume, Japan

*Correspondence to:*
Keisuke Hino, M.D., Ph.D.
Department of Hepatology and Pancreatology, Kawasaki Medical University
577 Matsushima, Kurashiki, Okayama, 701-0192, Japan
Tel: 81-86-4621111
Fax: 81-86-4641196
Email: khino@med.kawasaki-m.ac.jp

## ABSTRACT

We report a patient with alcoholic liver cirrhosis who had a 15 mm focal nodular hyperplasia (FNH)-like nodule in the liver. This FNH-like nodule was diagnosed as hepatocellular carcinoma (HCC) mainly based on hypervascularity during the hepatic arterial phase, washout pattern during the equilibrium phase and low signal intensity during the hepatobiliary phase in gadolinium-ethoxybenzyl-diethylenetriamine pentaacetic acid (Gd-EOB-DTPA)-enhanced MRI; it was surgically resected. Its histology exhibited hepatocyte hyperplasia, fibrous septa containing unpaired small arteries accompanied by reactive bile ductules, remarkable iron deposits and sinusoidal capillarization, and was compatible with the diagnosis of an FNH-like nodule. When we analyzed the images of the present nodule retrospectively, low signal intensity on in-phase and isosignal intensity on opposed-phase T1-weighted MRI may have reflected iron deposits in the FNH-like nodule. In addition, a low signal intensity on T2-weighted MRI and no detection in diffusion-weighted MRI may help in distinguishing FNH-like nodules from HCC, since these image findings are inconsistent with typical HCC. Immunohistochemical analysis revealed a markedly reduced expression of organic anion transporter (OATP) 1B3 in this nodule, which implied decreased Gd-EOB-DTPA uptake by hepatocytes and accounted for the low signal intensity during the hepatobiliary phase on Gd-EOB-DTPA-enhanced MRI. To the best of our knowledge this is the first report in which an FNH-like nodule was assessed for OATP1B3 expression.

**KEYWORDS**: alcoholic liver cirrhosis, FNH-like nodule, hepatocellular carcinoma, organic anion transporter, Gd-EOB-DTPA-enhanced MRI

## INTRODUCTION

Due to improvements in imaging techniques and pathological evaluation, a new type of small focal lesion occurring in the cirrhotic liver has been described (1-3). Focal nodular hyperplasia (FNH)-like nodules (FNH-like nodules) are focal lesions occurring in liver cirrhosis and are morphologically very similar to classical FNH in the otherwise normal liver. In general, FNH-like nodules are assumed not to have an increased risk of malignant transformation (1-3), but this issue remains elusive (4). FNH-like nodules are occasionally misdiagnosed on imaging as hepatocellular carcinoma (HCC) due to hypervascularity during the arterial phase of magnetic resonance imaging (MRI)/ computed tomography (CT).

On the other hand, gadolinium-ethoxybenzyl-diethylenetriamine pentaacetic acid (Gd-EOB-DTPA)-enhanced MRI has enabled us to detect focal liver lesions because of its hepatocyte-specific properties (5-7), and it might be the most useful imaging modality for the diagnosis of HCC at present (8, 9). However, the image findings of FNH-like nodules in Gd-EOB-DTPA-enhanced MRI are not well known, and it remains unclear if FNH-like nodules can be distinguished from HCC in Gd-EOB-DTPA-enhanced MRI. Here, we report a histologically proven FNH-like nodule in a patient with alcoholic liver cirrhosis, and discuss the diagnostic potential of Gd-EOB-DTPA-enhanced MRI for FNH-like nodules.

## CASE REPORT

A 68-year-old Japanese man with a history of alcoholic liver cirrhosis for approximately 10 years was found to have a 9 mm hypervascular nodule in the liver through contrast-enhanced CT and admitted to Kawasaki Medical University Hospital in June 2008 for further examination of the hepatic nodule.

His alcoholic consumption over the previous 40 years was 100 g or more per day. A physical examination on admission showed no remarkable abnormalities except for moderate splenomegaly. Laboratory data on admission disclosed the following abnormal values: platelet count $9.4\times10^4/\mu L$ (normal range 15-35), aspartate aminotransferase 58 IU/L (10-35), γ-glutamyl transpeptidase 346 IU/L (5-60) and indocyanine green retention rate at 15 minutes 16.4% (<10). The levels of hepatic tumor markers were as follows: α-fetoprotein 9.0 ng/mL (<10) and des-γ-carboxy prothrombin 25 mAU/mL (<40). The serum was negative for anti-hepatitis C virus antibody and hepatitis B surface (HBs) antigen but positive for anti-HBs and anti-hepatitis B core antibodies.

Neither B-mode sonographic scans nor Sonazoid contrast-enhanced ultrasonography detected the hepatic nodule. Arteriography did not disclose any hypervascular mass lesion. Contrast-enhanced CT revealed a nodule of 9 mm in the liver segment 3 as hypervascularity during the hepatic arterial phase.

Gd-EOB-DTPA-enhanced MRI disclosed that this nodule had a low signal intensity before contrast injection (Fig. 1A), hypervascularity during the hepatic arterial phase (Fig. 1B), a washout pattern during the equilibrium phase (Fig. 1C), and a low signal intensity during the hepatobiliary phase (Fig. 1D). Diffusion-weighted MRI did not reveal this nodule (Fig. 2A). In- and opposed-phase T1-weighted MRI, and T2-weighted MRI disclosed this nodule as low signal intensity (Fig. 2B), isosignal intensity (Fig. 2C) and slightly low signal intensity (Fig. 2D), respectively. Although this nodule was detected as slightly low signal intensity (Fig. 2E) in superparamagnetic iron oxide (SPIO)-enhanced MRI, it was uncertain if Kupffer cells took up SPIO because of the slightly low signal intensity on T2-weighted MRI before SPIO injection.

The imaging findings mentioned above were suggestive of HCC, even though several findings, such as low signal intensity on in-phase and isosignal intensity on

opposed-phase T1-weighted MRI, low signal intensity in T2-weighted MRI and no detection in diffusion-weighted MRI, were not consistent with typical HCC. We could not histologically assess this hepatic nodule by liver biopsy because of its undetectability by ultrasonography, and we could not ignore the possibility of HCC as the diagnosis of this nodule. Therefore, this nodule was surgically resected after obtaining informed consent from the patient. The nodule of interest was not encapsulated and its margin was difficult to distinguish from the surrounding cirrhotic tissue (Fig. 3A and 3B). Intranodular fibrous septa were present but central fibrous scarring and portal tracts were absent (Fig. 3C). The fibrous septa contained unpaired small arteries accompanied by reactive bile ductules radiating into the parenchyma (Fig. 3D). This nodule showed varying degrees of increased cellularity (Fig. 4A) and marked iron deposits in the hepatocyte and/or Kupffer cells (Fig. 4B) compared to the surrounding cirrhotic tissue. Immunohistochemical analysis using an anti-CD34 antibody (anti-CD34) revealed marked sinusoidal capillarization (Fig. 4C). Thus, the histological diagnosis of this nodule was an FNH-like nodule. Finally, we immunohistochemically assessed the expression of organic anion transporter (OATP) 1B3 in hepatocytes, using an anti-OATP1B3 antibody (anti- OATP1B3) to examine why this nodule exhibited low signal intensity during the hepatobiliary phase of Gd-EOB-DTPA-enhanced MRI. Immunohistochemically, OATP1B3 was diffusely and strongly positive for the cell membrane of the hepatocytes in the surrounding cirrhotic tissue, but was nearly absent in the FNH-like nodule (Fig. 5A-C). Thus far neither recurrence of the FNH-like nodule nor the development of HCC has been found in this patient who has stopped drinking alcohol since he was admitted to our hospital.

## DISCUSSION

FNH-like nodules occurring in cirrhotic livers are reported to have the pathological features such as encapsulation, hepatocyte hyperplasia, fibrous septa containing unpaired small arteries accompanied by reactive bile ductules, iron deposits and/or sinusoidal capillarization (1, 2). It has been suggested that the artery-dominant condition derived from disturbed portal circulation in the cirrhotic liver (10) or the congenital vascular anomaly (11, 12) causes localized hyperplastic changes of the hepatocytes, and generates nodular lesions such as FNH. The increased unpaired arteries, diffuse capillarization, and iron deposits in the nodule would be attributable to a similar mechanism in nodular formation. The FNH-like nodule in this study had these pathological features except for encapsulation. One possible explanation for the lack of encapsulation is that hepatocytic hyperplasia had not expanded sufficiently to be encapsulated because it was the early stage in the development of the hyperplastic nodule. In this respect the state of the present FNH-like nodule may suggest its early stage. The present case clearly indicated the existence of an FNH-like nodule with reduced OATP1B3 expression. Hepatocytic disorder derived from disturbed portal circulation in cirrhotic liver may have suppressed the expression of OATP1B3. We cannot necessarily exclude a possibility of malignant potential of this nodule in terms of nearly absent expression of OATP1B3. Otherwise, unknown mechanisms may have been related to the reduced expression of OATP1B3.

FNH-like nodules also are clinically important lesions in terms of difficulty in distinguishing them from well-differentiated HCC in image diagnosis. There were at least two reasons why we had diagnosed this patient as having probable HCC in imaging. First, the present FNH-like nodule exhibited hypervascularity during the hepatic arterial phase and a washout pattern during the equilibrium phase in contrast-enhanced MRI. Second, the Gd-EOB-DTPA-enhanced MRI revealed this nodule to have low signal intensity during the hepatobiliary phase, which implied reduced uptake of Gd-EOB-DTPA by hepatocytes. Reduced Gd-EOB-DTPA uptake by hepatocytes was reported to suggest an early event of hepatocarcinogenesis in a recent study (13). In contrast, FNH is demonstrated to be enhanced during the hepatobiliary phase of Gd-EOB-DTPA-enhanced MRI (5, 14). With respect to this point, it should be

noted that the present FNH-like nodule may have had an exceptionally low signal intensity during the hepatobiliary phase. The present results were consistent with the recent report that uptake of Gd-EOB-DTPA is determined by OATP1B3 expression rather than by tumor differentiation or bile production in HCC (15), and suggested the difficulty in discriminating between FNH-like nodules and HCC by assessing the Gd-EOB-DTPA uptake by hepatocytes.

Which MRI imaging findings were useful for distinguishing between FNH-like nodules and HCC in this patient? When we analyzed the images of this nodule retrospectively, there seemed to be three important findings for diagnosis. First, the low signal intensity on in-phase and isosignal intensity on opposed-phase T1-weighted MRI may have reflected iron deposits in the FNH-like nodule, since similar phase-shift imaging has been reported to reflect hemosiderin deposits in regenerative nodules in liver cirrhosis (16). In contrast, the isointensity to slightly high intensity on in-phase and the low signal intensity on opposed-phase T1-weighted MRI are known to reflect hepatocellular nodules with fatty degeneration (8). Thus, the combined findings from the in-phase and opposed-phase may facilitate discrimination between FNH-like nodules and well-differentiated HCC, since the former frequently have iron deposits and the latter has fatty degeneration. Second, FNH-like nodules and HCC have been shown to be likely to exhibit iso- to low signal intensity and high signal intensity in T2-weighted MRI, respectively (17), which was consistent with the low signal intensity in the present nodule. Third, the lack of detection in diffusion-weighted MRI may help in distinguishing FNH-like nodules from HCC, since diffusion-weighted MRI imaging has been reported to be useful in differentiating benign hepatocellular nodules including FNH from HCC (18). However, it still may be difficult to distinguish such small FNH-like nodules showing low signal intensity during the hepatobiliary phase in Gd-EOB-DTPA-enhanced MRI from HCC in clinical practice.

In addition, it remains controversial whether FNH-like nodules can be distinguished from HCC based on the presence of Kupffer cells in the nodules. A defect in the Kupffer phase on contrast-enhanced ultrasonography, which implies the absence of Kupffer cells, has been reported in the FNH-like nodule in alcoholic liver cirrhosis (19), whereas the presence of Kupffer cells on SPIO-enhanced MRI has also been

shown in FNH-like nodules in alcoholic liver cirrhosis (17). The present FNH-like nodule may have contained Kupffer cells, since Sonazoid contrast-enhanced ultrasonography did not detect this nodule. However, we could not precisely assess the uptake of SPIO by Kupffer cells because of the slightly low signal intensity on T2-weighted MRI before SPIO injection. Thus, the present case suggests the importance of pathological diagnosis for hepatic small nodular lesions as well as the difficulty in image diagnosis for such lesions. We also propose that observational follow-up is also an important modality to be chosen when nodules are less than 1.5 cm in diameter, since small nodular lesions associated with chronic liver diseases smaller than 1.5 cm have been reported to have less potential to be early HCC (20).

In conclusion, we found an FNH-like nodule with reduced expression of OATP1B3 in a patient with alcoholic liver cirrhosis, and retrospectively analyzed imaging findings useful for distinguishing FNH-like nodules from HCC.